



Transition from linear to nonlinear flow in single rough fractures: effect of fracture roughness

Jie Liu¹ · Zhechao Wang¹ · Liping Qiao¹ · Wei Li¹ · Jinjin Yang¹

Received: 11 May 2020 / Accepted: 17 December 2020 / Published online: 21 January 2021
© Springer-Verlag GmbH Germany, part of Springer Nature 2021

Abstract

A series of laboratory experiments on water flow through rough fractures was performed using self-designed experimental devices to investigate the effect of fracture roughness on the flow behavior. Nine models of single rough fractures—with three joint roughness coefficients (JRCs) of 0–2, 8–10 and 18–20, and three apertures for each JRC—were prepared using three-dimensional printing technology. In the flow experiments, the values of Reynolds numbers ranged widely from less than 10 to around 10,000. According to the experimental data, the fracture roughness has an obvious influence on the hydraulic properties of fractures. A parametric expression for the Forchheimer equation was proposed to quantitatively describe the influence of fracture roughness on the flow behaviour in the fractures. The relations between the parameters for nonlinear flow (such as critical Reynolds number, non-Darcy effect coefficient and friction factor) and the JRCs were obtained. It was found that the critical Reynolds number decreased significantly from 566 to 67 as the JRC increased from 2 to 20. The increase in fracture roughness causes more extra energy losses and enhances the degree of flow nonlinearity in single fractures.

Keywords Rough fracture · Nonlinear flow · Laboratory experiments · Forchheimer equation · Hydraulic properties

Introduction

Understanding the flow characteristics in fractured rock mass is of great importance to numerous rock engineering projects such as underground oil storage (Qiao et al. 2017; Wang et al. 2015), hydropower engineering (Chen et al. 2016), and contaminant pollution control (Qian et al. 2011). For many engineering applications, especially in hard rocks, fluid flow through fracture networks often dominates the overall flow pattern, which mainly depends on the geometry and connectivity of the fracture networks and on the hydro-mechanical coupling (Berkowitz 2002; Jing and Stephansson 2007). Single fractures are the main component of fracture networks in rock mass (Liu et al. 2016a). An adequate characterization of flow in single fractures is the foundation to better

understanding the hydraulic behavior of complex fractured rock mass.

The flow characteristics in single fractures were studied through experiments, numerical simulation or theoretical analysis in many previous studies (Berkowitz 2002; Scesi and Gattinoni 2007; Skjetne et al. 1999; Zimmerman and Bodvarsson 1996). The nonlinear flow characteristics in single fractures were usually a focused issue (Javadi et al. 2014; Jiang et al. 2008; Liu et al. 2016b). The research on fluid flow in fractures found that flow rate and hydraulic gradient generally conform to a linear relation at relatively low hydraulic gradients, but a nonlinear relation easily occurs in natural fractures at high hydraulic gradients (Chen et al. 2015a; Konzuk and Kueper 2004; Qian et al. 2011, 2018; Tzelepis et al. 2015; Zhou et al. 2016; Zimmerman et al. 2004). Geometric parameters such as fracture roughness, shear displacement, fracture filling and contact conditions, and fracture aperture, have great influence on the hydraulic characteristics of fractures (Javadi et al. 2014; Liu et al. 2017; Neuman 2005; Zimmerman and Bodvarsson 1996). Fracture roughness and shear displacement usually induce nonlinear flow in rock fractures or enhance the degree of flow nonlinearity (Liu et al. 2020; Tzelepis et al. 2015; Zhou et al. 2016, 2018). In the studies of nonlinear flow in fractures, the critical Reynolds

✉ Zhechao Wang
wang_zhechao@hotmail.com

¹ Key Laboratory of Ministry of Education on Safe Mining of Deep Metal Mines, Northeastern University, No. 11, 3rd Ave, Wenhua Rd, Shenyang 110004, Liaoning, China

number Re_c is often used to define the start of nonlinear flow (Liu et al. 2016b; Yu et al. 2017). The Re_c values in relevant research are distributed in a wide range from 0.001 to 2300 (Brush and Thomson 2003; Chen et al. 2015a; Qian et al. 2011; Zhou et al. 2016, 2018; Zimmerman et al. 2004). A comparison of studies on flow in single fractures is given in Table 1. The values of Re_c used in these studies range from 0.9 to 1000.

In the experiments on flow in fractures as listed in Table 1, smooth plexiglass plates (Qian et al. 2011; Zimmerman et al. 2004), split rocks (Javadi et al. 2014; Qian et al. 2018; Zhou et al. 2016), or plates with relative roughness attained by setting asperities on the wall (Tzelepis et al. 2015) were usually used to fabricate the fracture model. Tzelepis et al. (2015) analyzed the influence of relative roughness on flow characteristics in fractures. Qian et al. (2018) studied the flow characteristics in fractures with different joint roughness coefficients (JRCs) under high values of Re . In the research of Tzelepis et al. (2015) and Qian et al. (2018), the higher the roughness of the fracture, the higher the friction factor λ . Javadi et al. (2014) and Zhou et al. (2018) studied the influence of shearing processes on the nonlinearity of fluid flow.

The influence of fracture roughness on flow characteristics was mostly analyzed qualitatively in the studies compared in Table 1 (Qian et al. 2018; Tzelepis et al. 2015; Nigon et al. 2019). The surface geometry of fracture models made by plexiglass plates was quite different from that of actual rock fracture walls. The roughness of the fractures formed by split rocks was generally within limited ranges such as $JRC = 6$ – 12.6 (Zhou et al. 2016) and $JRC = 11.2$ – 14.51 (Qian et al. 2018). The Re values in the previous studies were also usually within limited ranges, such as $Re = 1$ – 30 (Zimmerman et al. 2004), $Re = 0.1$ – 13 (Zhou et al. 2016) and $Re = 900$ – $8,000$ (Qian et al. 2018). Given the difficulty in experiments, the studies on the flow characteristics in fractures under a wide range of Reynolds numbers yielded inconclusive results and are rarely reported in the literature.

In this study, laboratory flow experiments on artificial fractures with representative JRCs were conducted to

quantitatively evaluate the effect of fracture roughness on transition from linear to nonlinear flow. Based on the experimental results, a parametric expression for the Forchheimer equation, considering the fracture roughness, was proposed. The hydraulic properties of single rough fractures with a wide range of Reynolds numbers were investigated.

Experimental methodology

Experimental device

According to the experimental scheme, the experimental device for fluid flow was designed and fabricated as shown in Fig. 1. The experimental device mainly consists of four units: (1) water supply unit, (2) flow-rate measurement unit, (3) pressure measurement unit, and (4) data-processing unit. The water supply unit could provide a very stable water pressure of up to 1.2 MPa with fluctuations less than 0.01 MPa to keep the fluid flow as a steady state. High-accuracy turbine flowmeters (accuracy of $\pm 1.0\%$) and pressure sensors (accuracy of $\pm 0.5\%$) were fitted. All the turbine flowmeters and pressure sensors were calibrated manually to ensure the accuracy of experimental data. The data-processing unit could automatically record the flow rate, water pressure and water temperature once per second. The pipeline was made of stainless steel, and exhaust valves were arranged in the middle of the pipeline to remove any air in the pipeline. A filter was installed in the pipeline to keep the experimental water clean and to eliminate the effects of impurities on the sensors and the fracture model.

Fracture model preparation

The JRC is a well-known criterion for explicitly measuring roughness of rock fractures (Barton and Choubey 1977) and can be calculated by an empirical equation correlated with fracture wall slope (Tse and Cruden 1979). Thus, typical rough profiles with representative JRCs of 0–2, 8–10 and 18–20 (Barton and Choubey 1977) were used to represent

Table 1 Comparison of studies on flow in single fractures

Study (reference)	Method	Model size (mm), (length \times width)	Aperture (mm)	Roughness	Re_c	Model preparation
Zimmerman et al. 2004	Experiment and simulation	20 \times 20	0.15	Rough	10	Plexiglass plates
Qian et al. 2011	Experiment	1000 \times 250	4.0–9.0	Smooth	12–86	Plexiglass plates
Javadi et al. 2014;	Experiment	180 \times 100	Initially close	Rough	0.001–25	Split rock
Tzelepis et al. 2015	Experiment	6000 \times 500	3.0–13.0	Rough/smooth	200–1,000	Plexiglass plates
Zhou et al. 2016	Experiment	100 \times 50	0.002–0.08	JRC = 6–12.5	0.9–11.6	Split rock
Qian et al. 2018	Experiment	200 \times 100	0.5–2.0	JRC = 11.2–14.5	–	Split rock
Zhou et al. 2018	Simulation	Length 100	1.0	Relative roughness 0–0.4	40–145	Scanning split rock

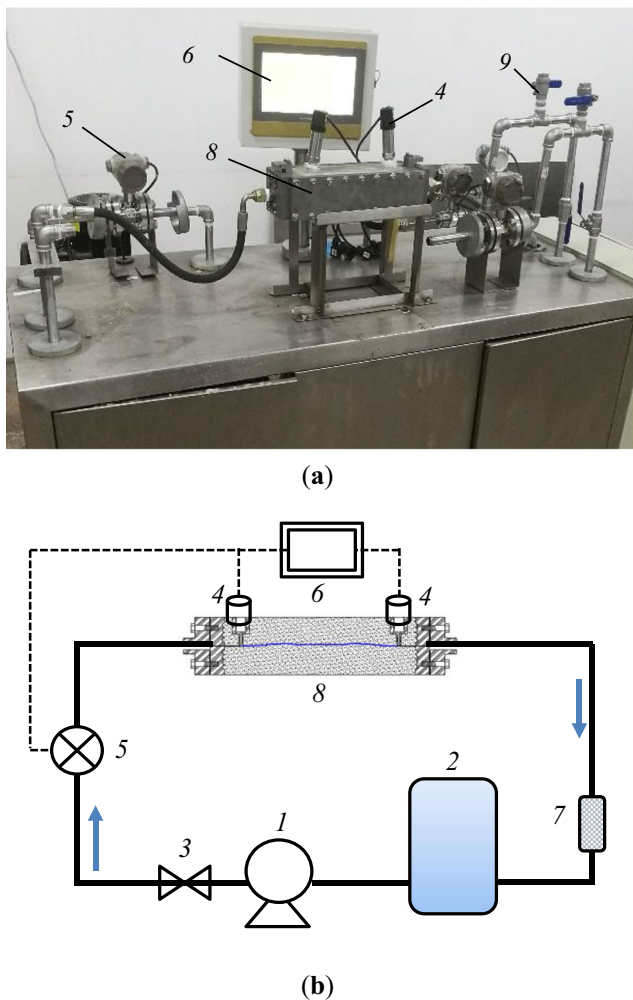


Fig. 1 a Experimental device and b schematic diagram for fluid flow in fractures. Legend: 1 pump, 2 water tank, 3 control valve, 4 pressure sensor, 5 turbine flowmeter, 6 data display, 7 filter, 8 fracture model, 9 exhaust valves

the fracture surfaces from smooth to rough, as shown in Fig. 2. The roughness parameter Z_2 , defined as the root mean square of the first derivative of the profile, and the mean asperity height R_m were calculated by Eqs. (1) and (2), respectively (Tse and Cruden 1979; Wang et al. 2016).

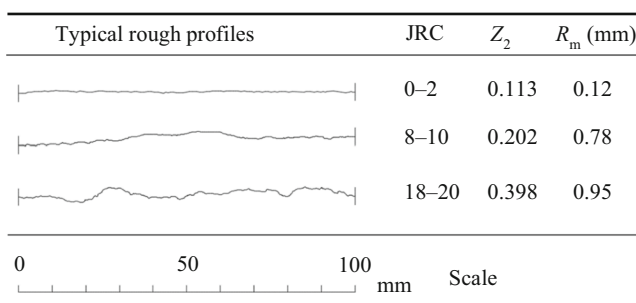


Fig. 2 Typical rough profiles with representative JRCs

$$Z_2 = \sqrt{\frac{1}{(n-1)(\Delta x)^2} \sum_{i=1}^{n-1} (\xi_{i+1} - \xi_i)^2} \quad (1)$$

$$R_m = \frac{1}{n} \sum_{i=1}^n |\xi_i - \xi_m| \quad (2)$$

where Δx is the sampling interval with the value between 0.4 and 0.5 mm, n is the number of sampling points, ξ_i is the asperity height of the i th sampling point, ξ_m is the mean line of asperity heights.

The fracture models with representative roughness were made with cement that could well represent the actual rough surfaces of rock fractures. First, coordinate curves were plotted according to the typical rough profiles of JRCs, and the two identical curves were symmetrically connected to form a curve of 200 mm length. A rough surface of 50 mm width was formed by the vertical translation of the JRC curves. Then a 3D model with the representative JRC of 50 mm width and 200 mm length was generated, and was printed as a template made of polylactic acid (PLA) using 3D printing technology, as shown in Fig. 3. The template was assembled with a stainless-steel model frame.

A schematic diagram and the fabrication process of the rough fracture models are shown in Figs. 4 and 5, respectively. The cement mortar was made of Portland cement, fine sand and anti-leakage additives to satisfy the requirements of strength, impermeability and geometric accuracy of the fracture model. As shown in Fig. 5a, the lower part of the fracture model was made by pouring the mortar into the assembled mould with the 3D printing template as the bottom board. After 2 days of curing, the lower part of the fracture model was turned over and the printing template was removed. Then the rough surface of the lower part was used as the bottom board of the mould to make the upper part of the fracture model, as shown in Fig. 5b. The mortar was poured into the mould with two metal piezometric holes embedded at both ends of the fracture model, as shown in Fig. 5c. After another 2 days of curing, the lower and upper parts of the fracture model were separated. In this way, the upper and lower surfaces of the fracture could be completely mated, and between which the vertical distance was equal everywhere. As shown in Fig. 5d, a 50-mm-long flat plate transition zone was arranged at both ends of the fracture; therefore, the fluid flow through the fracture was uniformly spread out along the flow direction in the fracture plane as assumed by the cubic law.

The rough-surface geometry of each fracture model was obtained (Fig. 6) using 3D laser scanning with the z -direction resolution of 0.02 mm. The mean intervals of the scanning points on the fracture surface were about 0.3 mm. As shown in Fig. 6, from the comparison between the scanning profile curves and the targeted fracture profiles with JRC = 18–20, the rough surface of the fracture models matched



Fig. 3 3D printing template with typical rough profile (JRC = 8–10)

well with the targeted profiles, indicating that the fracture models fabricated by the methods proposed in this article had high geometric accuracy.

To ensure the sealing of the fracture model, antileakage grooves were arranged on the mould, and sealants and silicone gaskets were installed around the model as shown in Figs. 4 and 5. The antileakage grooves with curved surface increased the contact area between the cement and the metal frame to prevent water leakage. Fifty-six screws were used to reinforce the model frame with high stiffness to prevent deformation of fractures during the experiments.

A total of nine fracture models were prepared with three fracture roughness coefficients (JRCs = 0–2, JRCs = 8–10, JRCs = 18–20), and three apertures were set for each fracture roughness coefficient. The geometrical and hydraulic parameters of the fracture models are listed in Table 2. The hydraulic apertures were back-calculated using the cubic law based on the experimental data, with the linear relation between flow rates and hydraulic gradients at relatively low flow rates. The average geometric apertures were obtained by measuring the geometric apertures of the fracture inlet and outlet using the feeler gauge. As it was very difficult to directly measure the geometric apertures of fracture models accurately, the geometric apertures were measured to preset the fracture apertures and as references to be compared with the hydraulic apertures in this study. The hydraulic apertures were used as aperture parameters in the experimental analysis. As shown in Table 2, the differences between geometric and hydraulic apertures were small. Probably due to measurement errors, the geometric apertures were smaller than the hydraulic apertures for some fracture models.

Experimental procedures

The laboratory flow experiments on rough fractures were performed at a room temperature of 20–21 °C. The density of the water was 998.2 kg/m³, the dynamic viscosity was 1.00×10^{-3} N · s/m², and the gravitational acceleration was 9.8 m/s². The water was considered to be incompressible, and the matrix was assumed to be impermeable. The flow rates were adjusted gradually by setting the water-supply pressure of the pump from 0.001 to 1.0 MPa and regulated by the control valve. During the experiments, the fluctuations of flow rates were usually less than 0.001 m³/h, so the fluid flow could be considered stable. The flow rate, water pressure at the inlet and outlet of the fracture, and water temperature could be

continuously displayed and recorded. There was a small range of pressure drop (less than 0.01 MPa) and flow rate (less than 0.04 m³/h), which were beyond the measuring range of the sensors. In order to improve the measurement accuracy, the pressure drop was measured by piezometer tubes, and the flow rate was calculated by measuring the mass of passing water in 1 or 2 min using an electronic balance with a precision of 0.01 g.

Experimental results

Relations between hydraulic gradient and flow rate

The cubic law is a commonly used equation to describe the linear flow in fractures that can be conceptualized as two smooth parallel plates. The cubic law has been verified theoretically and experimentally and is expressed as follows (Iwai 1976; Konzuk and Kueper 2004):

$$Q = \frac{\rho g w e_h^3}{12\mu} J \quad (3)$$

where Q is flow rate (m³/s), ρ is fluid density (kg/m³), g is gravity acceleration (m/s²), w is the fracture width (m), e_h is the fracture hydraulic aperture (m), μ is the dynamic viscosity (N · s/m²), and J is hydraulic gradient in the direction of water flow.

Based on the experimental data in this study, the relations between hydraulic gradient J and flow rate Q for flow in rough fractures are shown in Fig. 7. The values of Re ranged from less than 10 to around 10,000 and the maximum values of hydraulic gradient for each case ranged from 60 to 100. As shown in Fig. 7a, the roughness had a significant influence on the hydraulic properties of the rough fractures. The higher the JRC of a fracture, the higher the hydraulic gradient along the fracture was for a specified flow rate.

As shown in Fig. 7, especially Fig. 7c, when the flow rates were relatively low, the relation between flow rate and hydraulic gradient obeyed the cubic law well (i.e., the dotted lines, labeled ‘CL’ in the legends). As the flow rates increased gradually, the hydraulic gradients were significantly higher than the predicted values using the cubic law. The hydraulic gradient was found to be highly nonlinear with the flow rate at high flow rates in all the experiments.

To describe the nonlinear flow in fractures quantitatively, a widely used empirical equation referred to as the Forchheimer equation was developed in the form of Eq. (4) (Forchheimer 1901; Bear 1972):

$$J = A Q + B Q^2 \quad (4)$$

where A and B are the linear and nonlinear coefficients, respectively, describing energy losses due to viscous and inertial

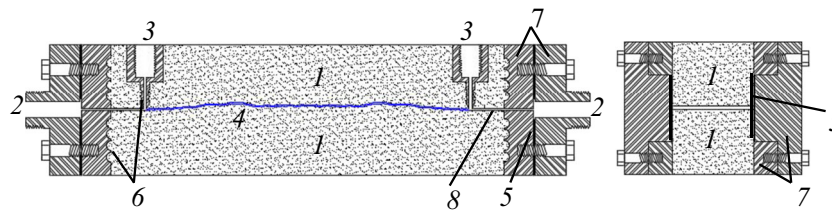


Fig. 4 Schematic diagram of the rough fracture model. Legend: 1 upper and lower parts of the cement fracture model, 2 inlet and outlet, 3 piezometric hole, 4 rough fracture, 5 silicone gasket and sealant, 6 anti-leakage groove, 7 stainless steel frame, 8 flat transition zone

dissipation mechanisms (Javadi et al. 2014). The Forchheimer equation has been proved to provide an excellent description for nonlinear flow behavior in fractures and is a typical model in the study of nonlinear flow.

The Forchheimer equation Eq. (4) was used to best fit the experimental Q - J curves. The predictions are shown by the solid lines in Fig. 7b–d. The coefficients of determination (R^2) of all the curves are very close to 1 ($R^2 > 0.997$), which indicates that the Forchheimer equation adequately describes the nonlinear flow behavior in single fractures.

Non-Darcy coefficient

With the parametric expressions of the parameters A and B , the Forchheimer equation is commonly written as (Chen et al. 2015b):

$$J = \frac{12\mu}{\rho g w e_h^3} Q + \frac{\beta}{g w^2 e_h^2} Q^2 \quad (5)$$

where β [L^{-1}] is the non-Darcy coefficient. A has an explicit expression inversely proportional to the cube of hydraulic aperture. Non-Darcy coefficient β is a key parameter in the expression of the Forchheimer equation and is important in describing the role of inertial forces in non-linear flow behavior in fractures.

The parameters A and B for all cases were calculated and fitted based on Eqs. (5) and (4), respectively. Then β could be calculated, and the results are listed in Table 3. Figure 8 shows

the relations between the non-Darcy coefficient and the hydraulic apertures. The non-Darcy coefficient increased obviously with the JRC values, indicating that fracture roughness would cause more nonlinear head loss of fluid flow in fractures.

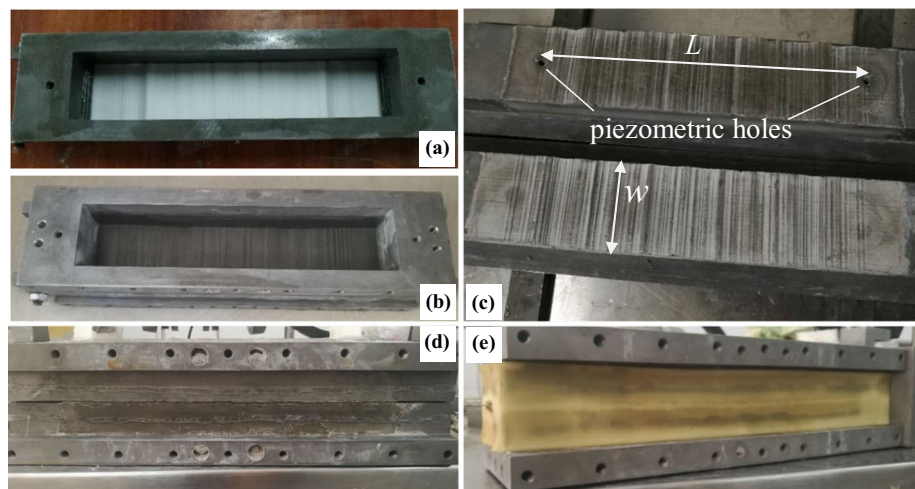
Generally, the non-Darcy coefficient is assumed to be mainly affected by fracture roughness (Zeng and Grigg 2006; Xu et al. 2012), so it should have remained constant in the cases with the same roughness. However, in cases 3 and 6 with greater apertures, and in cases 7–9 with higher roughness, the non-Darcy coefficient appears to fluctuate. Therefore, the experimental results suggest that the expression of coefficient B in Eq. (5) may be more capable of describing the flow behavior in fractures with smaller hydraulic apertures and lower JRCs.

The parametric expression of parameter B in Eq. (5) was reexamined by modifying the parametric expression. Considering the influence of the fracture-sidewall on flow experiments, and for the dimension unity, the exponents of width w and hydraulic aperture e_h in Eq. (5) were modified to $(4-\alpha)$ and α . The modified parametric expression of coefficient B was proposed as follows:

$$B = \frac{\beta}{g w^{4-\alpha} e_h^\alpha} \quad (6)$$

The best-fitted values of α for the three sets of cases with different JRCs were obtained, and they are shown in Table 4.

Fig. 5 Fabrication process of the experiment fracture model: **a** pouring the lower fracture model, **b** pouring the upper fracture model, **c** rough fracture surface, **d** applying sealant, **e** adhering silicone gasket



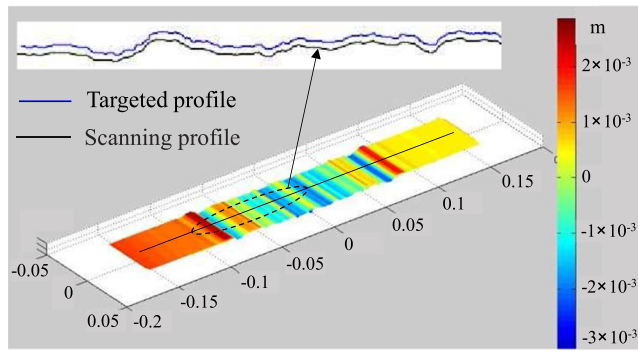


Fig. 6 Rough surface geometry of the fracture model by 3D laser scanning (JRC = 18–20; unit, m)

The average value of α was 2.3. Then the value of β for each case was redetermined according to Eq. (6). The obtained values of β based on Eq. (6) for the cases with the same JRCs were more consistent than the fitted values based on Eq. (5). After modification of the parametric expression, the coefficient β values were mainly affected by the fracture roughness.

The average values of β for the cases with the same JRCs were calculated. By analyzing the variation of average values of β with JRCs, and considering the upper and lower limits of the JRCs, a hyperbolic tangent function in the form of Eq. (7) was used to describe the relation between β and the JRCs:

$$\beta = a \times \tanh(b \times \text{JRC}) + c \tag{7}$$

where the parameters $a = 18.09$, $b = 0.038$, $c = 1.06$ in Eq. (7) were obtained by best-fit regression analyses with $R^2 = 0.998$, as shown in Fig. 9. Then the limiting values in the range of the JRCs were obtained: $\beta = 1.06$ for a smooth fracture with $\text{JRC} = 0$, and $\beta = 12.57$ for the roughest fracture with $\text{JRC} = 20$. Eq. (7) could predict the non-Darcy coefficient β for fractures with different JRCs. The expression for the Forchheimer

equation that could quantitatively describe the influence of fracture roughness on flow behavior in fractures can be written as:

$$J = \frac{12\mu}{\rho g w e_h^3} Q + \frac{a \times \tanh(b \times \text{JRC}) + c}{g w^\alpha e_h^{4-\alpha}} Q^2 \tag{8}$$

Transition from linear to nonlinear flow

In order to predict the onset of nonlinear flow behavior and represent the nonlinearity of flow in fractures, the Reynolds number Re and the non-Darcy effect E have been commonly employed (Skjetne et al. 1999; Zeng and Grigg 2006; Javadi et al. 2014; Yu et al. 2017). The Reynolds number is defined as the ratio of inertial forces to viscous forces for fluid flow. For fluid flow in fractures, Re is generally expressed as (Konzuk and Kueper 2004; Zhang and Nemcik 2013b):

$$Re = \frac{2\rho Q}{\mu w} = \frac{2\rho v e_h}{\mu} \tag{9}$$

where v is the flow velocity.

The non-Darcy effect is defined as the ratio of the nonlinear pressure drop to the total pressure drop in Eq. (4), which can be written as (Zeng and Grigg 2006):

$$E = \frac{BQ^2}{AQ + BQ^2} \tag{10}$$

E is strictly in the range of 0–1 indicating the transform of flow regimes from laminar flow to fully developed turbulent flow. The critical value of E is usually taken as 0.1, as a criterion for distinguishing the linear and nonlinear flow (Zeng and Grigg 2006; Yu et al. 2017; Zhang and Nemcik 2013a). According to this criterion, the corresponding critical Reynolds number Re_c , that defines the

Table 2 Geometrical and hydraulic parameters of the fracture models

Case No.	Length, L (mm)	Width, w (mm)	Geometric aperture, e_m (mm)	Hydraulic aperture, e_h (mm)	JRC
1	202.0	50.0	0.80	0.775	0–2
2	202.0	50.0	1.00	0.956	0–2
3	202.0	50.0	1.32	1.365	0–2
4	201.0	50.0	0.56	0.596	8–10
5	201.0	50.0	0.80	0.811	8–10
6	201.0	50.0	1.20	1.182	8–10
7	200.0	50.0	0.42	0.393	18–20
8	200.0	50.0	0.70	0.697	18–20
9	200.0	50.0	0.95	0.885	18–20

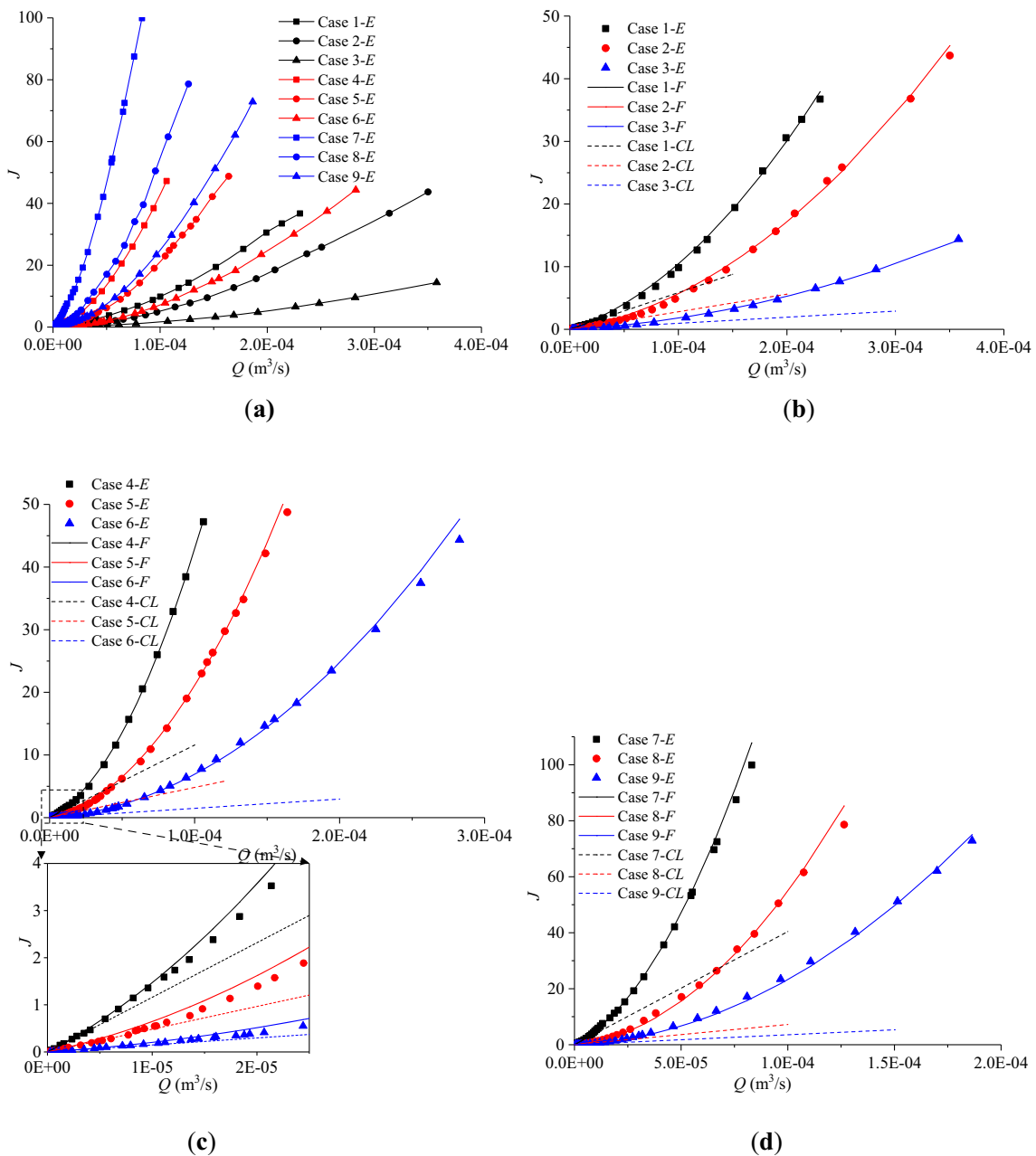


Fig. 7 The relation between hydraulic gradient J and flow rate Q (In the legend, E experimental result, F fitted result, CL cubic law). **a** Experimental results, **b** JRC = 0–2, **c** JRC = 8–10, **d** JRC = 18–20

Table 3 Calculated and fitted parameters of each experiment case

Case No.	A	B	R^2	β
1	5.86×10^4	4.59×10^8	0.998	6.75
2	2.81×10^4	2.89×10^8	0.996	6.47
3	9.65×10^3	8.38×10^7	0.998	3.83
4	1.16×10^5	3.12×10^9	0.999	27.19
5	4.83×10^4	1.63×10^9	0.999	26.26
6	1.48×10^4	5.44×10^8	0.999	18.61
7	4.04×10^5	1.17×10^{10}	0.997	44.45
8	7.25×10^4	4.76×10^9	0.998	56.67
9	3.54×10^4	1.97×10^9	0.998	37.76

start of nonlinear flow, can be determined by Eqs. (9) and (10), as expressed in Eq. (11) (Zimmerman et al. 2004; Yu et al. 2017):

$$Re_c = \frac{2\rho AE}{\mu w B(1-E)} = \frac{2\rho A}{9\mu w B} \tag{11}$$

As shown in Fig. 10, which displays the critical Reynolds number of each experiment case, the roughness has a significant influence on the values of the critical Reynolds numbers. The values of Re_c ranged from 431 to 566 for JRC = 0–2. As the roughness increased, the values of Re_c decreased

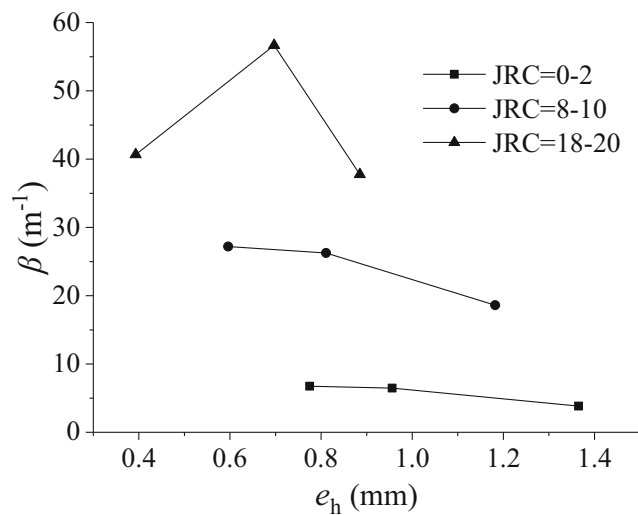


Fig. 8 The relation between non-Darcy coefficient β and hydraulic aperture e_h

significantly and ranged from 67 to 153 for JRC = 18–20. Therefore, the higher the roughness, the more likely it is to cause nonlinear flow.

According to Eqs. (8) and (11), the parametric expression of the critical Reynolds number, considering fracture roughness, was obtained as follows:

$$Re_c = \frac{2\rho AE}{\mu w B(1-E)} = \frac{8}{3[18.09 \tanh(0.038JRC) + 1.06] w^{0.3} e_h^{0.7}} \quad (12)$$

The relation between non-Darcy effect E and Re of each case is shown in Fig. 11. It was noted that the non-Darcy effect increased obviously with JRC values for a specified Reynolds number. With the increase of fracture roughness, the tortuosity of the flow paths increased and led to more head loss caused by inertial force. With the increase of Re , the non-Darcy effect increased gradually or even approached 1, which indicated that the nonlinearity of flow was getting stronger and the nonlinear head loss caused by inertial force accounted for the main sector of the total head loss. For example, at $Re = 5,000$, the nonlinear term of head loss accounted for about 90% of total head loss in cases 8 and 9.

Table 4 Fitted parameters of α and β (α : the exponent of hydraulic aperture e_h)

Case Nos.	JRC	α , fitted	α , average	β , Eq. (6)	β , average
1, 2, 3	0–2	2.65	2.3	1.93, 1.97, 1.30	1.74
4, 5, 6	8–10	2.32	2.3	7.20, 7.62, 6.05	6.96
7, 8, 9	18–20	1.81	2.3	9.51, 15.72, 11.26	12.16

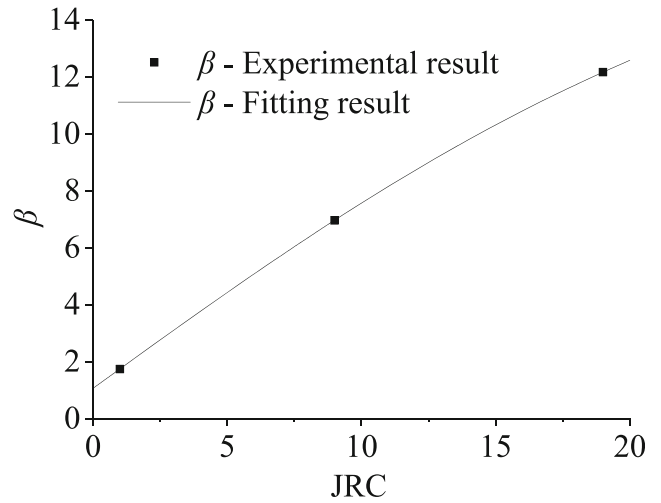


Fig. 9 The relation between non-Darcy coefficient β and values of the joint roughness coefficient (JRC)

Friction factor of nonlinear flow

For fluid flow in fractures, friction factor λ represents the degree of water head loss caused by the resistance along the flow path. The friction factor is expressed as the Darcy-Weisbach equation (White 2003):

$$J = \lambda \frac{1}{D_h} \frac{v^2}{2g} \quad (13)$$

where $D_h = 2e_h$ is the equivalent hydraulic diameter of the fracture, and the hydraulic gradient J represents the total energy losses. According to Eqs. (3), (9) and (13), the expression of the friction factor for linear flow that only considers the viscous forces was obtained as follows:

$$\lambda = \frac{48\mu w}{\rho Q} = \frac{96}{Re} \quad (14)$$

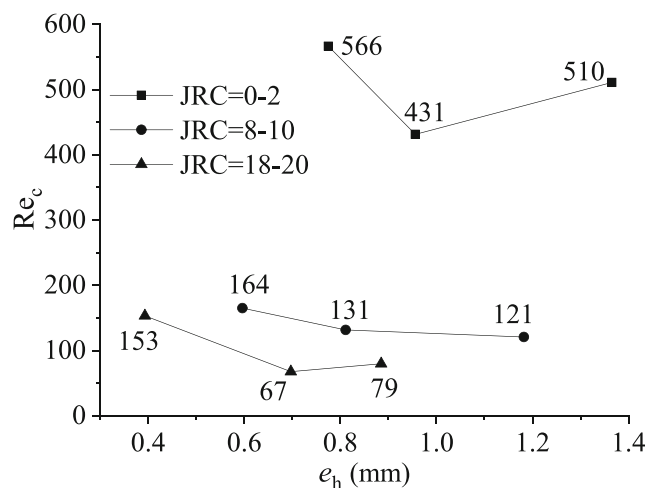


Fig. 10 Critical Reynolds number Re_c of each experiment case

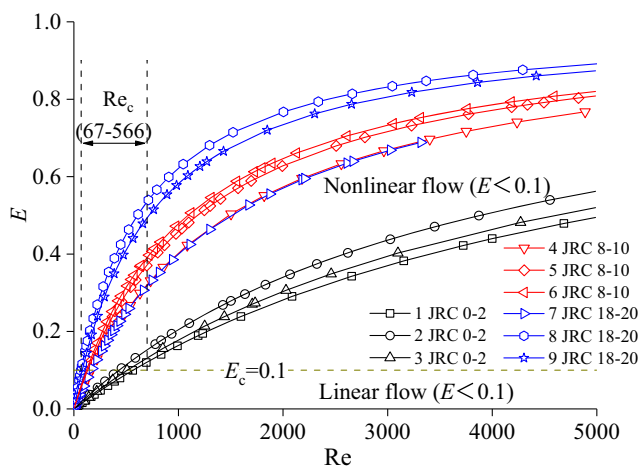


Fig. 11 The relation between non-Darcy effect E and Reynolds number Re

Based on Eqs. (8) and (13), the parametric expression of the friction factor for nonlinear flow was obtained as follows:

$$\lambda = \frac{96}{Re} + 4\beta w^{0.3} e_h^{0.7} \tag{15}$$

where the right terms $96/Re$ and $4\beta w^{0.3} e_h^{0.7}$ represent two parts of the friction factor caused by the viscous and the inertial forces, respectively. Based on the experimental results, the relation between the friction factor and Re was obtained, and is shown in Fig. 12. In the linear flow regime with $Re < Re_c$, the friction factors for each case were consistent with that obtained by the Eq. (14), indicating that the energy losses were mainly caused by viscous forces. In the nonlinear flow regime with $Re > Re_c$, the friction factor is higher than that predicted by Eq. (14) because of the extra energy losses due to inertial forces. And the friction factor increased obviously with the JRCs. The experimental results implied that fracture roughness had a greater influence on the nonlinear flow regime than on the linear flow regime, because the tortuosity of

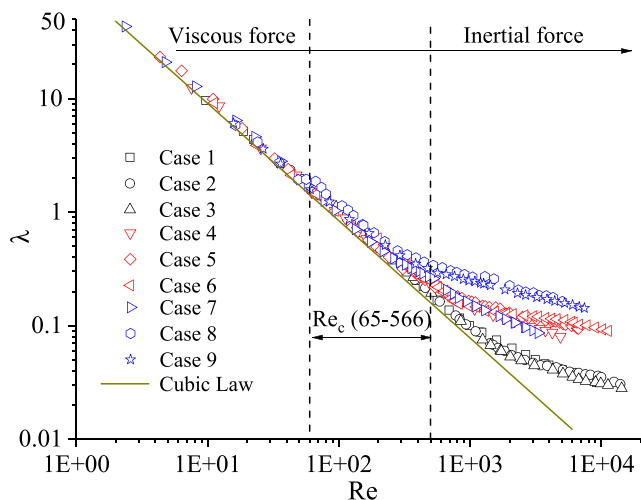


Fig. 12 The relations between friction factor λ and Re of the experiments

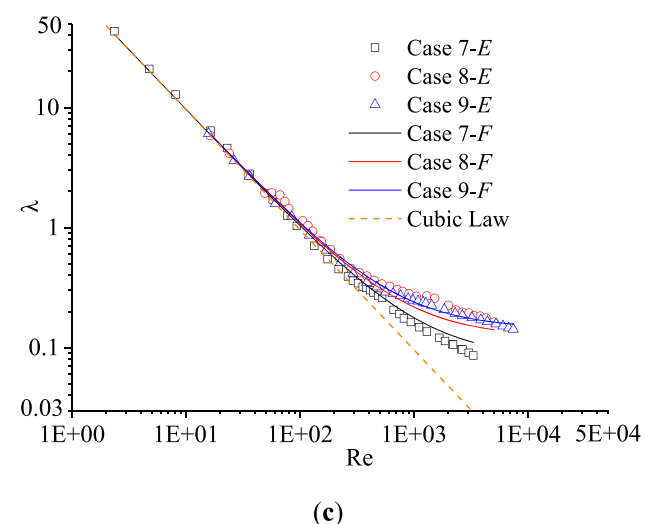
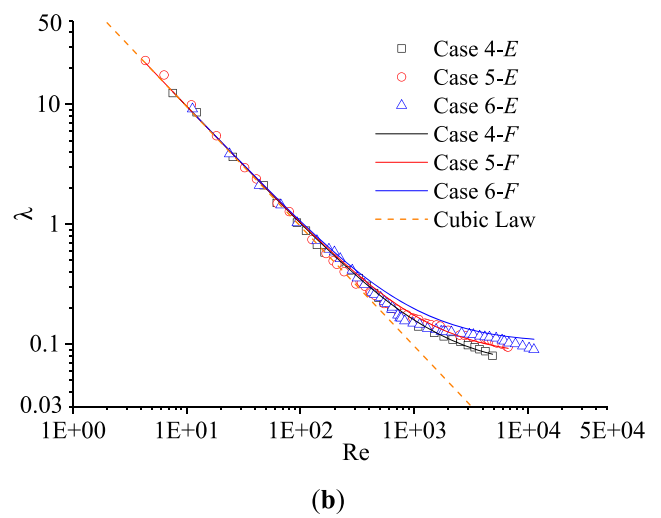
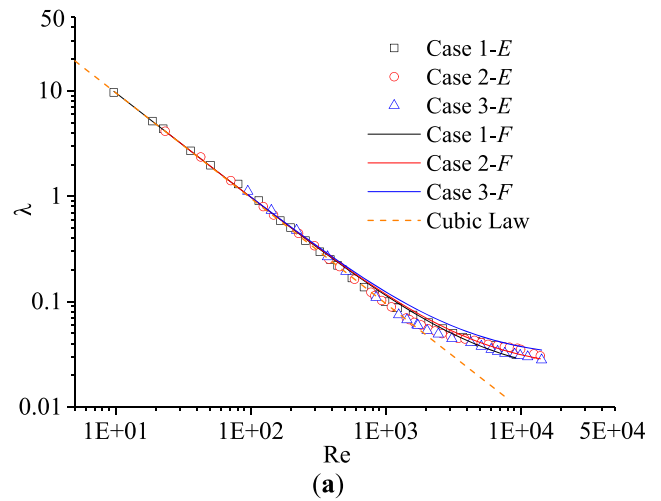


Fig. 13 Comparison of friction factor λ between experimental and fitted predicted results (Legend: E experimental result, F fitted predicted result). **a** JRC = 0–2) **b** JRC = 8–10 **c** JRC = 18–20

the flow path usually led to inertial energy losses in the nonlinear flow regime—for example, the friction factor λ of case

9 in the experiments is about 4 times that of case 2 at $Re = 5,000$.

The comparison of friction factors between the experimental results and predicted results using Eq. (15) is shown in Fig. 13, and the coefficients of determination R^2 of all cases were higher than 0.99. The nonlinear term $4\beta w^{0.3} e_h^{0.7}$ is constant, and when $Re < Re_c$, it is much smaller than the linear term $96/Re$ and can be ignored. As Re increases, $96/Re$ decreases sustainably and becomes smaller than $4\beta w^{0.3} e_h^{0.7}$; then $4\beta w^{0.3} e_h^{0.7}$ will account for the main part of the friction factor.

Conclusions

To investigate the characteristics of nonlinear flow in rough fractures, laboratory flow experiments were carried out using self-designed experimental devices with a wide range of Re values from less than 10 to around 10,000. It was found in the experiments that the hydraulic gradient is highly nonlinear with the flow rate in rough fractures. The roughness has a significant influence on the hydraulic properties of rough fractures and causes more inertial energy losses. The Forchheimer equation adequately describes the nonlinear flow behavior in single fractures with a wide range of Re . Based on the experimental data and regression analysis, a parametric expression for the Forchheimer equation was proposed that could quantify the influence of fracture roughness on flow behavior. The relation between non-Darcy coefficient β and JRCs was obtained, and β varied from 1.06 to 12.57 in the full range of JRCs.

The values of Re_c decreased significantly from 566 to 67 as the JRCs increased from 2 to 20. The higher the roughness, the more likely it is to cause nonlinear flow. The parametric expression of critical Reynolds number Re_c considering fracture roughness was obtained. With the increase of Re , the non-Darcy effect E increased gradually and even reached 0.9, indicating that the nonlinearity of flow was getting stronger. The experimental results of friction factor λ implied that fracture roughness had a greater influence on the nonlinear flow regime than on the linear flow regime, because the tortuosity of the flow path usually led to inertial energy losses in the nonlinear flow regime.

The results of this study provide solid evidence that the effects of fracture roughness and nonlinear flow on hydraulic properties of fractures should be paid more attention in the analysis of flow in fractured-rock engineering projects. For example, to ensure the containment properties of underground water-sealed oil storage caverns, the actual water head imposed on the storage caverns should be higher than that obtained using the common linear equation, due to the conclusion that the roughness and inertial forces would cause extra energy losses. The results also indicate that water discharge

into tunnels predicted using the linear Darcy equation may be overestimated, which has been reported in some studies, due to neglecting the nonlinear flow effect.

Funding This study was financially supported by the National Natural Science Foundation of China under contract Nos. 51779045 and 51579141, the Fundamental Research Funds for the Central Universities under contract Nos. N180104022 and N2001026, Liao Ning Revitalization Talents Program under contract No. XLYC1807029 and Liaoning Natural Science Foundation under contract No. 2019-YQ-02.

References

- Barton N, Choubey V (1977) The shear strength of rock joints in theory and practice. *Rock Mech* 10:1–54. <https://doi.org/10.1007/BF01261801>
- Bear J (1972) *Dynamics of fluids in porous media*. Elsevier, Amsterdam
- Berkowitz B (2002) Characterizing flow and transport in fractured geological media: a review. *Adv Water Resour* 25(8):861–884. [https://doi.org/10.1016/S0309-1708\(02\)00042-8](https://doi.org/10.1016/S0309-1708(02)00042-8)
- Brush DJ, Thomson NR (2003) Fluid flow in synthetic rough-walled fractures: Navier-Stokes, Stokes, and local cubic law simulations. *Water Resour Res* 39(4):1085. <https://doi.org/10.1029/2002WR001346>
- Chen YF, Hu SH, Hu R, Zhou CB (2015a) Estimating hydraulic conductivity of fractured rocks from high-pressure packer tests with an Izbash's law-based empirical model. *Water Resour Res* 51(4):2096–2118. <https://doi.org/10.1002/2014WR016458>
- Chen YF, Zhou JQ, Hu SH, Hu R, Zhou CB (2015b) Evaluation of Forchheimer equation coefficients for non-Darcy flow in deformable rough-walled fractures. *J Hydrol* 529:993–1006. <https://doi.org/10.1016/j.jhydrol.2015.09.021>
- Chen YF, Hong JM, Tang SL, Zhou CB (2016) Characterization of transient groundwater flow through a high arch dam foundation during reservoir impounding. *J Rock Mech Geotech Eng* 8(4):462–471. <https://doi.org/10.1016/j.jrmge.2016.03.004>
- Forchheimer PH (1901) Water movement through soil (in German). *J Assoc Ger Eng* 45:1782–1788
- Iwai K (1976) *Fundamental studies of fluid flow through a single fracture*. Ph D thesis, California University, Berkeley. [https://doi.org/10.1016/0148-9062\(79\)90543-6](https://doi.org/10.1016/0148-9062(79)90543-6)
- Javadi M, Sharifzadeh M, Shahriar K, Mitani Y (2014) Critical Reynolds number for nonlinear flow through rough-walled fractures: the role of shear processes. *Water Resour Res* 50(2):1789–1804. <https://doi.org/10.1002/2013WR014610>
- Jiang YJ, Li B, Wang G, Li SC (2008) New advances in an experimental study on seepage characteristics of rock fractures (in Chinese). *Chin J Rock Mech Eng* 27:2377–2386
- Jing L, Stephansson O (2007) *Fundamentals of discrete element methods for rock engineering: theory and applications*. Elsevier, Amsterdam. p 111–138
- Konzuk JS, Kueper BH (2004) Evaluation of cubic law based models describing single-phase flow through a rough-walled fracture. *Water Resour Res* 40(2):W02402. <https://doi.org/10.1029/2003WR002356>
- Liu RC, Jiang YJ, Li B, Yu LY, Du Y (2016a) Nonlinear seepage behaviors of fluid in fracture networks (in Chinese). *Rock Soil Mech* 37(10):2817–2824
- Liu RC, Yu LY, Jiang YJ (2016b) Quantitative estimates of normalized transmissivity and the onset of nonlinear fluid flow through rough rock fractures. *Rock Mech Rock Eng* 50(4):1–9. <https://doi.org/10.1007/s00603-016-1147-1>

- Liu RC, Jing HJ, He LX, Zhu TT, Yu LY, Su HJ (2017) An experimental study of the effect of fillings on hydraulic properties of single fractures. *Environ Earth Sci* 76:684. <https://doi.org/10.1007/s12665-017-7024-8>
- Liu RC, Huang N, Jiang YJ, Jing HW, Yu LY (2020) A numerical study of shear-induced evolutions of geometric and hydraulic properties of self-affine rough-walled rock fractures. *Int J Rock Mech Min Sci* 127:1–17. <https://doi.org/10.1016/j.ijmms.2020.104211>
- Neuman SP (2005) Trends, prospects and challenges in quantifying flow and transport through fractured rocks. *Hydrogeol J* 13(1):124–147. <https://doi.org/10.1007/s10040-004-0397-2>
- Nigon B, Englert A, Pascal C (2019) Three-dimensional flow characterization in a joint with plumose pattern. *Hydrogeol J* 27(1):87–99. <https://doi.org/10.1007/s10040-018-1847-6>
- Qian JZ, Zhan HB, Chen Z, Ye H (2011) Experimental study of solute transport under non-Darcian flow in a single fracture. *J Hydrol* 399(3):246–254. <https://doi.org/10.1016/j.jhydrol.2011.01.003>
- Qian X, Xia CC, Gui Y (2018) Quantitative estimates of non-Darcy groundwater flow properties and normalized hydraulic aperture through discrete open rough-walled joints. *Int J Geomech* 18(9):04018099. [https://doi.org/10.1061/\(ASCE\)GM.1943-5622.0001228](https://doi.org/10.1061/(ASCE)GM.1943-5622.0001228)
- Qiao LP, Wang ZC, Li SC, Bi LP, Xu ZH (2017) Assessing containment properties of underground oil storage caverns: methods and a case study. *Geosci J* 21(4):579–593. <https://doi.org/10.1007/s12303-016-0063-4>
- Scesi L, Gattinoni P (2007) Roughness control on hydraulic conductivity in fractured rocks. *Hydrogeol J* 15(2):201–211. <https://doi.org/10.1007/s10040-006-0076-6>
- Skjetne E, Hansen A, Gudmundsson JS (1999) High-velocity flow in a rough fracture. *J Fluid Mech* 383:1–28. <https://doi.org/10.1017/S0022112098002444>
- Tse R, Cruden DM (1979) Estimating joint roughness coefficients. *Int J Rock Mech Min Sci Geomech Abstr* 16(5):303–307. [https://doi.org/10.1016/0148-9062\(79\)90241-9](https://doi.org/10.1016/0148-9062(79)90241-9)
- Tzelepis V, Moutsopoulos KN, Papaspyros JNE, Tsihrintzis VA (2015) Experimental investigation of flow behavior in smooth and rough artificial fractures. *J Hydrol* 521(2):108–118. <https://doi.org/10.1016/j.jhydrol.2014.11.054>
- Wang ZC, Li SC, Qiao LP, Zhang QS (2015) Finite element analysis of hydromechanical behavior of an underground crude oil storage facility in granite subject to cyclic loading during operation. *Int J Rock Mech Min Sci* 73:70–81. <https://doi.org/10.1016/j.ijmms.2014.09.018>
- Wang M, Chen YF, Ma GW, Zhou JQ, Zhou CB (2016) Influence of surface roughness on nonlinear flow behaviors in 3D self-affine rough fractures: lattice Boltzmann simulations. *Adv Water Resour* 96:373–388. <https://doi.org/10.1016/j.advwatres.2016.08.006>
- White FM (2003) *Fluid mechanics*, 5th edn. McGraw-Hill, New York. p 304–314
- Xu K, Lei XW, Meng QS, Zhou XB (2012) Study of inertial coefficient of non-Darcy seepage flow (in Chinese). *Chin J Rock Mech Eng* 31(1):164–170
- Yu LY, Liu RC, Jiang YJ (2017) A review of critical conditions for the onset of nonlinear fluid flow in rock fractures. *Geofluids* 2017:1–17. <https://doi.org/10.1155/2019/9273968>
- Zeng Z, Grigg R (2006) A criterion for non-Darcy flow in porous media. *Transp Porous Media* 63(1):57–59. <https://doi.org/10.1007/s11242-005-2720-3>
- Zhang Z, Nemcik J (2013a) Fluid flow regimes and nonlinear flow characteristics in deformable rock fractures. *J Hydrol* 477(1):139–151. <https://doi.org/10.1016/j.jhydrol.2012.11.024>
- Zhang Z, Nemcik J (2013b) Friction factor of water flow through rough rock fractures. *Rock Mech Rock Eng* 46(5):1125–1134. <https://doi.org/10.1007/s00603-012-0328-9>
- Zhou JQ, Hu SH, Chen YF, Wang M, Zhou CB (2016) The friction factor in the Forchheimer equation for rock fractures. *Rock Mech Rock Eng* 49(8):3055–3068. <https://doi.org/10.1007/s00603-016-0960-x>
- Zhou JQ, Wang M, Wang LC, Chen YF, Zhou CB (2018) Emergence of nonlinear laminar flow in fractures during shear. *Rock Mech Rock Eng* 51:3635–3643. <https://doi.org/10.1007/s00603-018-1545-7>
- Zimmerman RW, Bodvarsson GS (1996) Hydraulic conductivity of rock fractures. *Transp Porous Media* 23(1):1–30. <https://doi.org/10.1007/bf00145263>
- Zimmerman RW, Al-Yaarubi A, Pain CC, Grattoni CA (2004) Nonlinear regimes of fluid flow in rock fractures. *Int J Rock Mech Min Sci* 41(3):163–169. <https://doi.org/10.1016/j.ijmms.2004.03.036>

Publisher's note Springer Nature remains neutral with regard to jurisdictional claims in published maps and institutional affiliations.